J. Water Environ. Nanotechnol., 7(1): 55-68 Winter 2022

ORIGINAL RESEARCH PAPER

Effective Methylene Blue Removal from Aqueous Solutions using PVA/Chitosan Electrospun Nanofiber Modified with $CeAlO_3$ Nanoparticles

Fatemeh Shahverdi, Aboulfazl Barati*, Mansour Bayat

Department of chemical engineering, Arak university, Arak, Iran

Received: 2021-10-15 Accepted: 2021-11-27 Published: 2022-02-01

ABSTRACT

This research work aims to investigate the sorption characteristic of synthesized Poly (vinyl alcohol)/Chitosan nanofiber mats modified with aluminum-cerium spinel oxide ($CeAlO_3$) nanoparticles for methylene blue (MB) removal from aqueous solutions. The sorption is carried out by a batch technique. The structural characterization of this nanocomposite was performed by Fourier transform infrared spectroscopy (FTIR) and X-ray diffraction analysis (XRD). Scanning electron microscopy (SEM) results showed uniform net and improved nanofibers with diameters ranging about 420 and 450 nm, respectively. The optimum conditions of MB removal onto modified PVA/CS nanofibers were found to be: pH 10, contact time 45 min, and 0.01 g of adsorbent in 400 ml in aqueous solution. Furthermore, the experimental adsorption data were in excellent agreement with the pseudo-second-order kinetics. The experimental results showed that there is a good correlation between the obtained data and the adsorption isotherm in the concentration range studied (400-600 mg/l). The results revealed that the maximum adsorption capacity of MB was 817.81 and 714.61 mg/g onto improved and net nanofibers, respectively.

Keywords: *Batch processing, Methylene blue, $CeAlO_3$, Isotherms, Kinetics*

How to cite this article

Shahverdi F., Barati A., Bayat M. Effective Methylene Blue Removal from Aqueous Solutions using PVA/Chitosan Electrospun Nanofiber Modified with CeAlO3 Nanoparticles. J. Water Environ. Nanotechnol., 2022; 7(1): 55-68.

DOI: 10.22090/jwent.2022.01.005

INTRODUCTION

Nowadays, with the rapid growth of population and increased industrialization, water pollution poses direct negative effects to the environment as well as on human life. Various water pollutants, including dyes, heavy metal ions, organics, and so on are of interest [1]. Among these, due to the toxicity and non-degradability of almost all dyes, the study of their removal from wastewater is very important. Methylene blue (MB), as one of the commonly known cationic soluble dyes, is used in different applications to protect materials and facilitate the sale or make goods more expensive. The most common MB effects are headache, dizziness, nausea, vomiting, dyspnea, and chest discomfort [2]. Therefore, eliminating the risk of trapping it in wastewater is of great interest to protect the health and safety of the environment [3]. In recent years, various processes such as coagulation/flocculation, chemical oxidation adsorption, and ultrafiltration have been widely used to remove dyes from wastewaters. Among these processes, adsorption has been investigated as the cost-effective method due to the high removal efficiency of dyes removal in low concentration and easy process [4]. Present electrospun nanofiber membrane with promising properties, such as fine diameters, high porosity, tunable pore size, and high surface to volume ratio is one of the most important recent researches [5]. The preparation of electrospun nanofibers from various polymers

* Corresponding Author Email: *a-barati@araku.ac.ir*

and biopolymers has been considered to utilize in different applications [6-11]. Chitosan is recognized as a natural and versatile biomaterial that the existence of hydroxyl and amino groups in its structure, making it a suitable biosorbent for organic dyes and heavy metal ions by chelation or electrostatic interaction [12]. Mahmoodi et al. carried out a study on anionic dyes removal from colored wastewater using crosslinked electrospun PVA/CS blend nanofiber by glutaraldehyde vapor. Their results showed that maximum uptake capacity was 151, 95, and 114 (mg/g) for Direct Red 80, Direct Red 81, and Reactive Red 180, respectively at pH 2.1 [13]. Other researchers studied the effect of ZIF-8@chitosan/PVA electrospun nanofibers dose on the removal of Malachite green dye and they found that the removal percentage increased with increasing the adsorbent dose of ZIF-8 and from results, the optimum of its dosage was 0.03 g/L [14]. Li et al. investigated the removal of acid blue-113 from an aqueous solution using electrospun chitosan nanofibers [15]. They found that the diameter of chitosan fibers has a considerable effect on the removal efficiency and by decreasing of nanofiber diameter from micro to nanoscale, the adsorption capacity increased from 412 to 1377 mg/g. Furthermore, providing conditions for optimal use of nano-sized powder adsorbents with high porosity can increase the efficiency of removing pollutants from industrial effluents. Among these nanomaterials, $CeAlO_3$ nanoparticle powders synthesized by combustion technique, are often spherical and have an average particle size of 14,068 nm. This polycrystalline powder is single-phase and due to its magnetic properties as well as its highly porous structure (Fig 1), it can be used in the process of removing contamination from aqueous solutions [16]. In this study, to obtain the optimum and smooth electrospun nanofibers structure, effective parameters such as voltage, distance to the collector, and feed rate of the electrospinning process were identified by the design of experiment (DOE). Then, the removal of methylene blue dye using prepared electrospun nanocomposite adsorbents that cross-linked by citric acid was investigated for the first time. The effects of pH value, contact time, and concentration on the process were studied. Also, sorption kinetics and isotherms properties of the process were obtained.

MATERIALS AND METHODS

Materials

In this study, polyvinyl alcohol with a molecular weight of 49,000 was obtained from Fluka. $CeAlO_3$ was prepared at Arak University (16). Triton x-114 was supplied by Applichem. Chitosan with a molecular weight of 100 KD and other high purity chemicals and solvents were purchased from Merck Company.

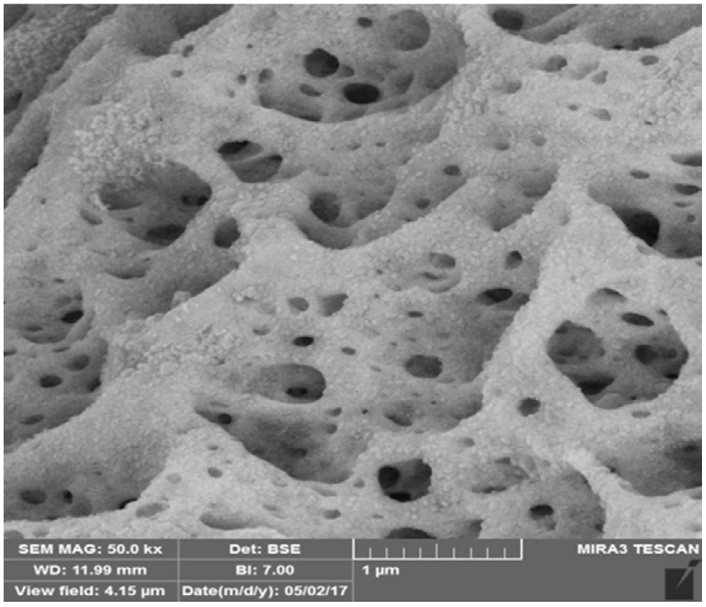

Fig. 1. TEM image of $CeAlO_3$ nanoparticle powders synthesized by combustion technique

Instrumentation

We used the electrospinning instrument (Nano Azma Co) for preparing nanofibers. The morphology of electrospun nanofibers was observed using a scanning electron microscope (SEM) (Beyond Technology, Korea) with a gold coating. Average diameters of nanofibers were measured by Digimizer.5.4.9 software. Fourier transform infrared spectroscopy (FTIR) analysis (Perkin Elmer) was used to investigate the structural changes using the KBr method. X-ray diffraction studies of nanocomposite samples were studied by X-ray diffractometer (Philips X-3064 Pert Pw) with Cr K-alpha-1 radiation source at ambient temperature. The pH of MB dye solution was adjusted by using HCl and NaOH and measured with a pH meter (Mi 180 Bench Meter). The residual MB concentration in the aqueous solution before and after the adsorption process was measured using a UV/ Vis spectrophotometer (Perkin-Elmar-lambada25).

Batch adsorption experiments

All experiments were done at room temperature to study the effects of experimental conditions such as pH, contact time, and the initial methylene blue concentration. The process was done by using appropriately diluted 500 ppm stock solutions. At the beginning of the experiment, the pH value of each dye test solution was adjusted by the addition of HCl and NaOH solutions. In each step, 0.01 g of the nanofibers was added to the samples and shaken with the rotating speed of 150 rpm (PIT10LO). For equilibrium studies, nanocomposite was put into dye solutions with initial concentrations ranging from 400 to 600 mg/l. The equilibrium time of the process was estimated by drawing samples at desired time intervals. MB solution was separated from the adsorbent by centrifugation (model), and the residual dye concentration in the solution was determined by a UV/Vis spectrophotometer. The amount of MB adsorbed per unit mass of nanocomposite (adsorption capacity) was calculated in the following equation:

$$q_{e=}\frac{V\left(C_{\circ}\_C_{e}\right)}{M}$$

where q_e is the equilibrium uptake (mg/g), C_0 and Ce are the initial and the equilibrium dye concentration (mg/L), respectively, V is the volume of the solution in contact with the nanocomposite (mL), and M is the mass of the added adsorbent (g) [17].

Experimental design

In this study, controllable factors including voltage, distance from the collector, and feed rate were designed in three levels. Central Composite Design (CCD) was used to determine the optimum experimental conditions for the synthesis of smooth surface and uniform nanofiber mats. According to Table 1, PVA/CS fibers were prepared uniformly only under one condition at voltage 18 kv, distance to collector 10 cm, and feed rate of 0.3 cm^3 /h with the diameter ranging about 381 nm.

Synthesis of the nanocomposite

Approximately 2 wt.% of chitosan was dissolved in concentrated acetic acid. 12 wt.% PVA solution was prepared by dissolving in deionized water. The solutions were prepared at a ratio of 1:1 at room temperature. Briefly, a clear aqueous solution of cerium nitrate, aluminum nitrate, and glycine based on the ratio stoichiometry of reactions [16] was prepared and then heated on a magnetic stirrer at 90 ° C for 1 hour. After a few seconds of the combustion reaction, all gases were released and $CeAlO_3$ nanoparticles $_{were}$ prepared in the powder. the PVA/CS blend was divided into two parts and About 1 wt.% of $CeAlO_3$ and 1% Triton x-114 were mixed in one of the PVA/CS parts to get PVA/CS/ $CeAlO_3$ blend while the other blend was used as a blank. Furthermore, 0.002 g of citric acid was added to both solutions to cross-link the fibers and stirred overnight. The solutions were used for electrospinning under optimum conditions. Then the prepared nanofibers dried and were cured in an oven at 140 °C for 2 h to initiate chemical crosslinking.

RESULTS AND DISCUSSION

Characterization of the adsorbents

Scanning electron microscopy (SEM) was used to investigate the prepared optimal nanofibers before and after cross-linking, and diameter distributions of the fibers are shown in Figs (1-4). It is seen that the net and improved nanofibers before cross-linking by citric acid are very smooth and uniform. However, after cross-linking, the surface of the fibers appears slightly rough, which may be due to the evaporation of existing water in the mats. Then, 100 fibers were analyzed with Digimizer software and the size distribution histograms of the nanofibers were drawn. The diameters of the net and improved nanofibers before and after cross-linking were 381, 420, 412, and 450 nm, respectively. The

Table.1. Design of experiment for preparing the nanofibers

Run	Voltage (kv)	Rate(cm^3 /h)	Distance(cm)	Diameter(nm)
1	19	0.2	11	No Fiber
2	20	0.2	11	No Fiber
3	19	0.2	11	No Fiber
4	20	0.3	10	No Fiber
5	18	0.3	12	No Fiber
6	20	0.1	10	No Fiber
7	19	0.2	11	No Fiber
8	18	0.2	11	No Fiber
9	18	0.1	10	No Fiber
10	19	0.1	11	No Fiber
11	18	0.3	10	Fiber
12	19	0.2	11	No Fiber
13	19	0.2	12	No Fiber
14	18	0.1	12	No Fiber
15	19	0.2	10	No Fiber
16	19	0.3	11	No Fiber
17	20	0.3	12	No Fiber
18	20	0.1	12	No Fiber
19	19	0.2	11	No Fiber

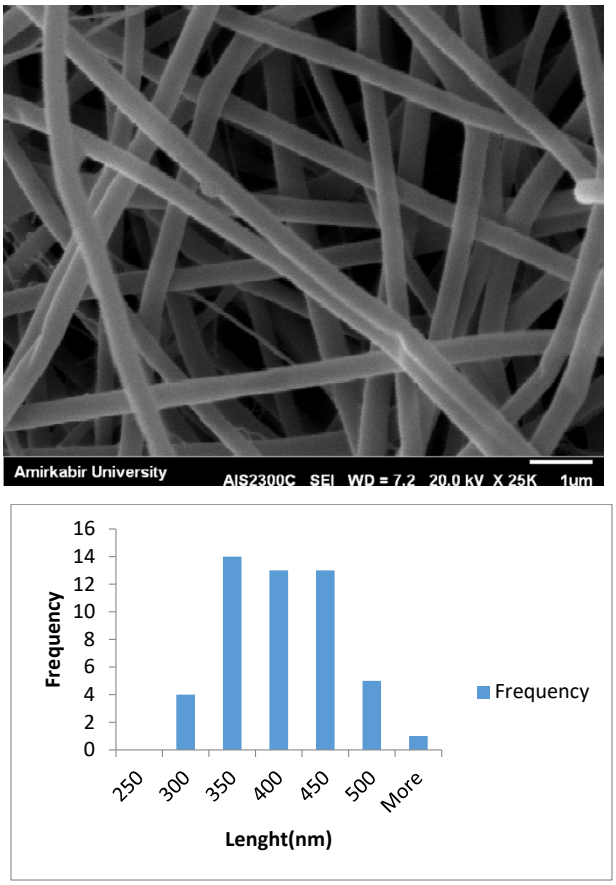

Fig. 2. SEM image of PVA/CS electrospun nanofibers before crosslinking process, average nanofibers diameter (381 nm)

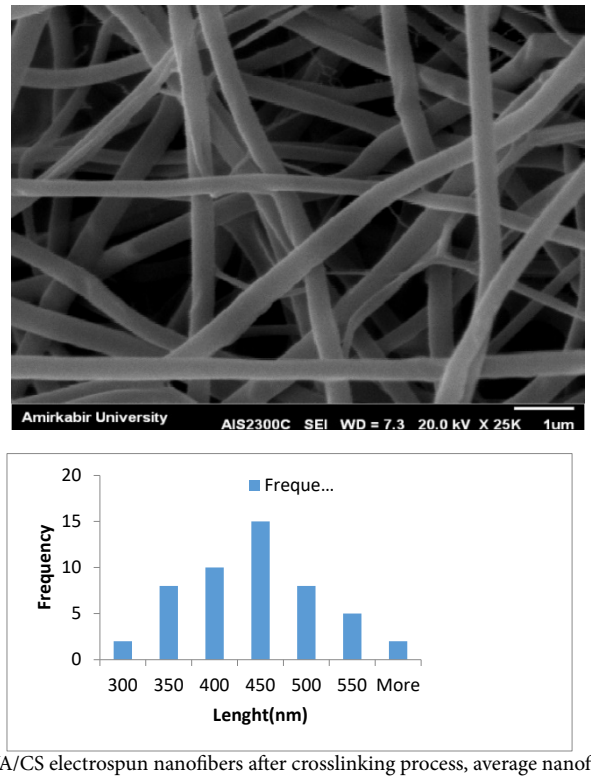

Fig. 3. SEM image of PVA/CS electrospun nanofibers after crosslinking process, average nanofibers diameter (420 nm)

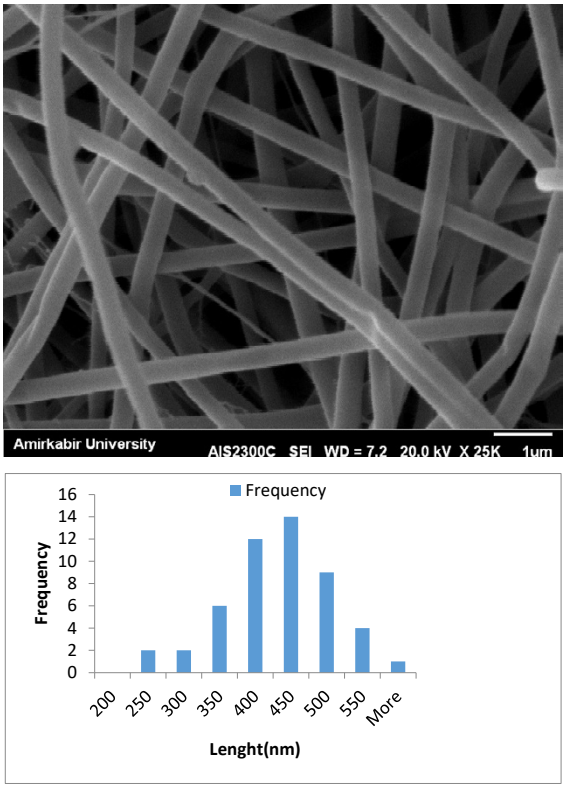

Fig. 4. SEM image of PVA/CS/ $CeAlO_3$ electrospun nanofibers before cross-linking process average nanofibers diameter (412 nm)

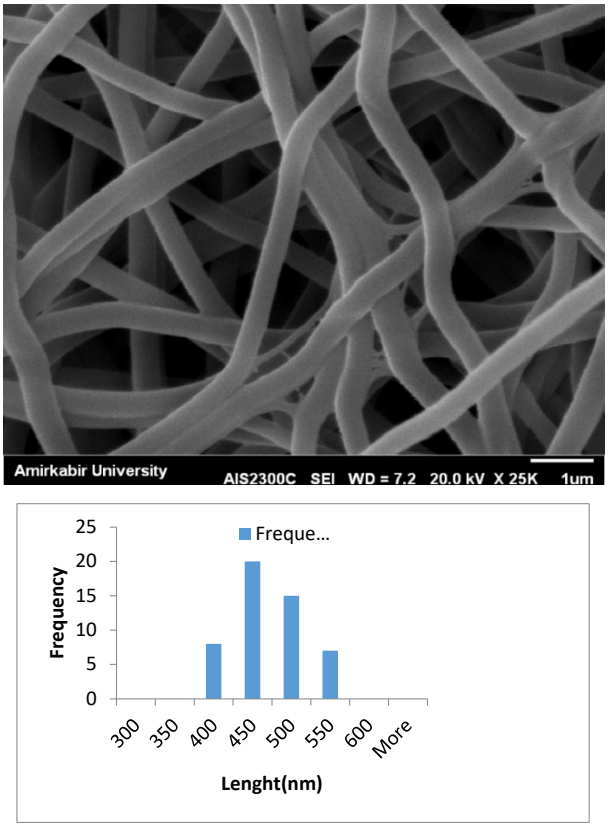

Fig. 5. SEM image of PVA/CS/ $CeAlO_3$ electrospun nanofibers after cross-linking process, average nanofibers diameter (450 nm)

viscosity of them increased by adding the citric acid and $CeAlO_3$ nanoparticles to the polymeric solutions. Therefore, as can be seen, the diameter of the average nanofibers is larger than the net PVA/CS nanofibers.

Fourier Transform Infrared Spectroscopy

In the spectra of CS/PVA before crosslinking (Fg.6a) the adsorption peak at 3312 cm−1 in it, which was wider than that in the spectra of cross-linked CS/PVA, the reason being that CS/PVA has more O–H groups than cross-linked CS/PVA. The band in the range of 3000–3700 cm−1, represented the overlapped stretching vibration of –OH and N–H in the CS and –OH in the PVA. Furthermore, for the cross-linked CS/PVA membrane (Fig. 6b), the peak of –OH/N–H of CS shifted from 3312 cm−1 to 3351 cm−1, which was due to the formation of hydrogen bonding between the hydroxyl in PVA and amino in CS and hydroxyl groups in citric acid. Fig. 6 presents a broad and strong peak at 3351 cm^{-1} assigned to -OH and N-H stretching, indicating the presence of hydroxyl and amino groups, respectively. 2939 cm^{-1} attributed to C-H stretching of Alkanes. 1734, 1567 are attributed to the C = O aldehyde, C = C stretching bonds of alkene, respectively. C-H scissor and bending belongs to 1426-1290 cm^{-1}. Also, 1511 and 832 cm^{-1} peaks belong to N-O stretching and C = C vibration bonds of alkene, respectively. 1328 and 1090 cm^{-1} are belonging to the C-O alcoholic and C-N stretching vibration of the chitin–chitosan and protein fractions. Fig. 6b indicates that the bands that have been observed at 3351, 2939, 1734, and 1090 cm^{-1} for adsorbent before process shifted to 3362, 2941, 1736, 1094 cm^{-1}, respectively (Fig. 6c). The significant changes in the wavenumbers of these specific peaks indicate that these bonds were effective in the methylene blue adsorption process [18].

As can be seen in the X-ray diffraction (Fig. 7), raw chitosan and polyvinyl alcohol powders revealed sharp peaks at (2θ=30.165) and (2θ =29.81) angles, respectively, indicating that the raw materials are crystalline. However, with the blend of these materials together, the intensity of the peaks and their crystallinity decreased. the reduction of the crystallinity of the nanofibers may be attributed

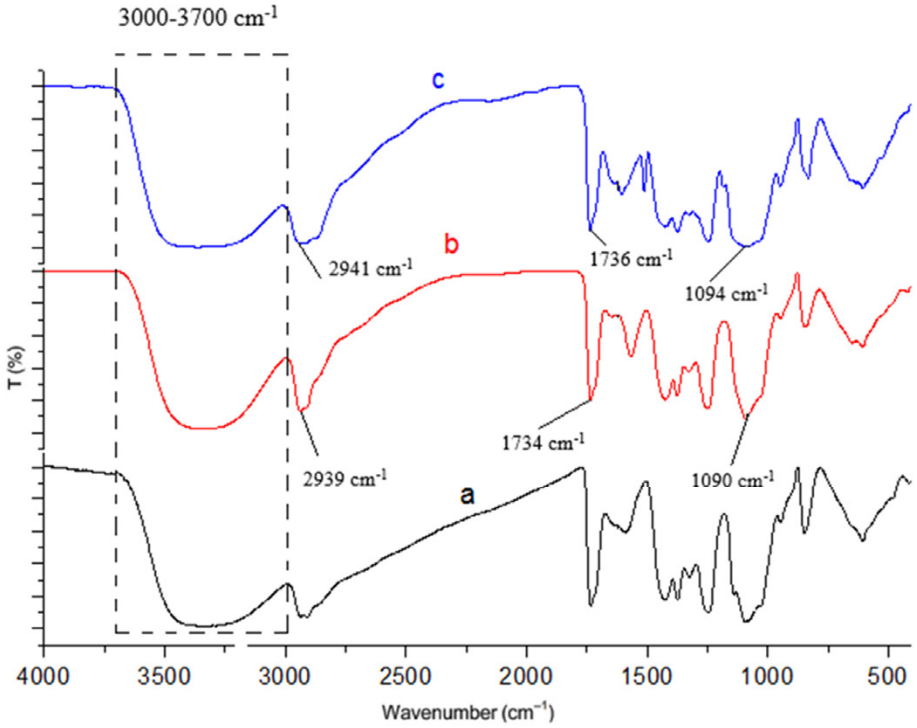

Fig. 6. FTIR spectrum of (a) PVA/CS/ $CeAlO_3$ nanofibers (b) cross-linked PVA/CS/ $CeAlO_3$ nanofibers before adsorption, (c) cross-linked PVA/CS/ $CeAlO_3$ electrospun nanofibers after adsorption

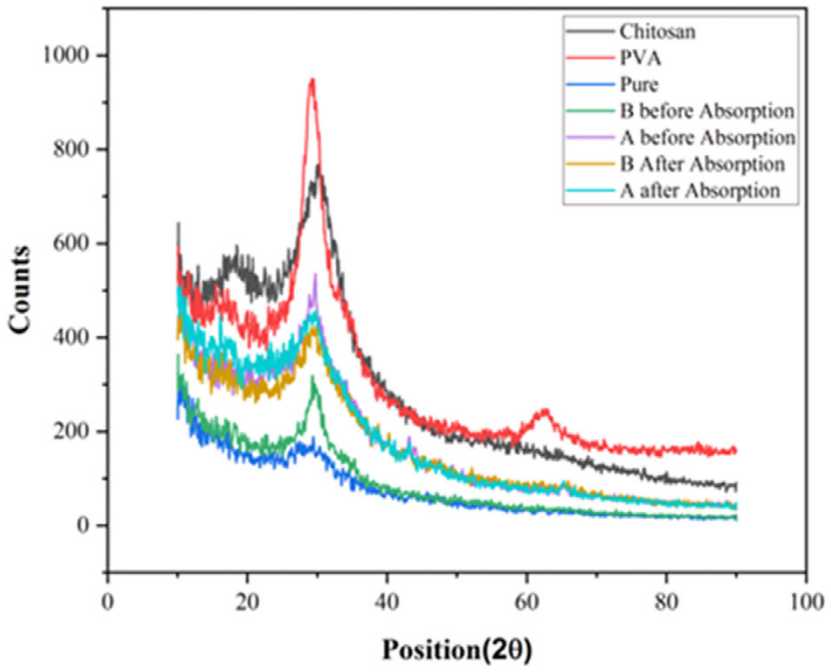

Fig. 7. XRD pattern of raw PVA, raw CS, pure PVA/CS, cross-linked PVA/CS/ $CeAlO_3$(A) and PVA/CS/ (B)

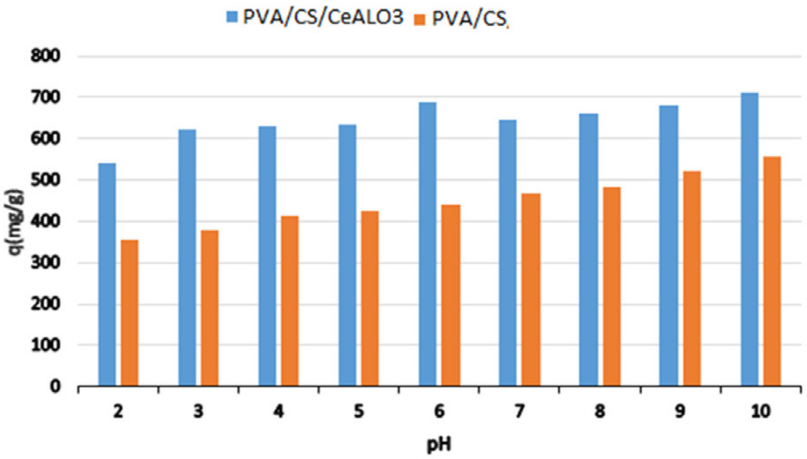

Fig. 8. Effect of pH on sorption of MB onto PVA/CS and PVA/CS/ $CeAlO_3$

to the hydrogen bonding interaction between molecules in the prepared mats. Furthermore, there were almost no obvious effects on the crystallinity of the nanofibers by the cross-linking process. With the addition of the $CeAlo_3$ nanoparticles to PVA/CS, the peaks are strongly increased (2θ= 29.5). After the adsorption, as can be seen, the PVA/CS/$CeAlo_3$ nanocomposite change in the crystallinity structure was less than the net PVA/CS nanofibers.

Effect of pH

The effect of pH of the solution on MB sorption using the nanocomposite from an aqueous solution was investigated in an initial pH range of 2 to 10. Experiments were done with constant concentration (400 mg / l) containing 0.01 g of the adsorbent at different pHs, at room temperature, and for 30 min on a shaker with 150 rpm. according to Fig. 8. As can be seen, with increasing pH, the adsorption capacity of both adsorbents has increased and has reached its maximum value at pH 10. It can be concluded that, at low pH values and acidic conditions of the solution, the dimethylamine groups in MB ions and amine groups in the adsorbent (chitosan) are protonated. Therefore, the electrostatic attraction between the positively charged adsorbent and the positively charged dye decreases. At higher pH conditions of the solution, hydrogen bonding and electrostatic interactions between MB ions and functional groups of nanocomposite during the adsorption process increases and lead to the improved adsorption of dye from aqueous solutions. The results are consistent with the other MB removal studies [19- 23].

Effect of contact time

In order to obtain the equilibrium time for the adsorption of MB, the process was investigated at different times Fig. (9). The operating conditions including contact time (180min) and optimum pH were constant for each adsorbent. As can be seen, at the beginning of the process, due to the availability of active sites and functional groups on the external surface, the adsorption of MB increased considerably with increasing contact time. Bypassing time, uptake capacity reduced with decrease of the interior active sites and it remained constant thereafter. According to the obtained results, the equilibrium time was considered to be 45 minutes for improvement and 90 minutes for the net adsorbent.

Kinetics of sorption

Proper prediction of batch sorption kinetics is necessary to optimum operating conditions and the design of industrial sorption systems. The adsorption kinetics was studied for a better understanding of the dynamics of MB removal and obtaining predictive models that allow estimations of the amount of adsorbed dye with the contact time. This information could be used for the scale-up to a larger system. The pseudo-first-order, pseudo-second-order kinetics, and intraparticle diffusion models were thus applied to the experimental data obtained (Figs. 10-12). The pseudo-second-order kinetics model, unlike the pseudo-first-order kinetics model, predicts adsorption behavior at all times of the adsorption process [24, 25]. The linear form of different kinetics is expressed in Equations 2 to 4 as follows:

$$\log(qe-qt)=\log qe - \frac{k1t}{2.303} \quad (2)$$

$$\frac{t}{qt}=\frac{t}{q_e}+\frac{1}{qe^2k_2} \quad (3)$$

$$q_t = k_{id}t^{.5}+c \quad (4)$$

Where, K_1 is the rate constant of the pseudo-first sorption kinetic $(min)^{-1}$, K_2 is the rate constant of the pseudo-second sorption kinetic ((g)/ (mg min)), k_{id} is intraparticle diffusion constant (mg/g $min^{-.5}$), and C is intraparticle diffusion constant (mg/g). Then, using the line equations obtained from plotting and matching it with the adsorption kinetics equations, the adsorption kinetics parameters were calculated (13). According to the results, intraparticle diffusion is not the rate-controlling step. The correlation coefficient factor, R^2, calculated from the pseudo-second-order model fits the experimental data very well with an amount of 0.99 for both adsorbents. The q_e value derived from the second-order model (769.23) for net nanofiber is more comparable with the

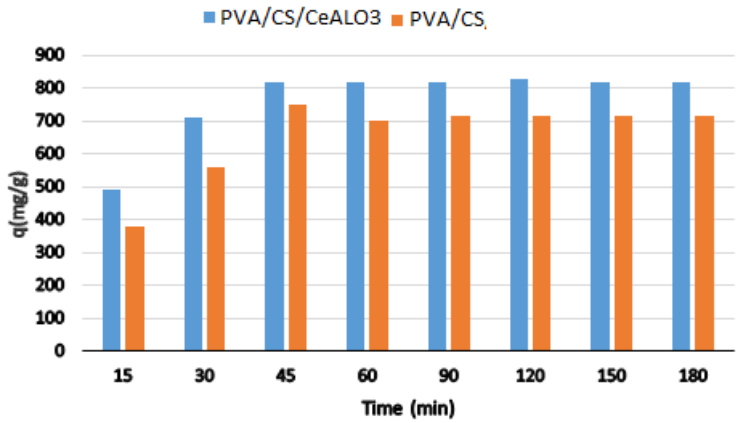

Fig. 9. Effect of contact time on sorption of MB onto PVA/CS and PVA/CS/ $CeAlO_3$

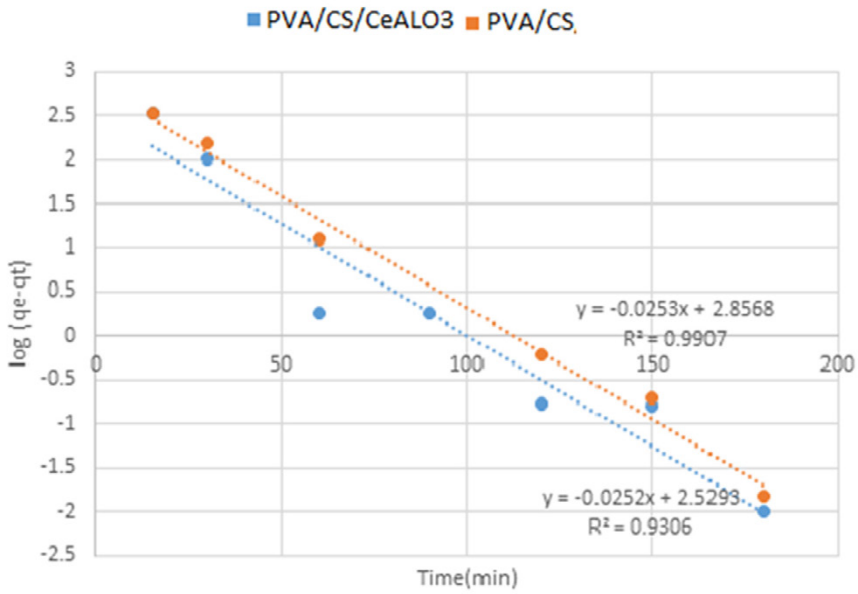

Fig. 10. Pseudo-first-order plot sorption of MB onto PVA/CS and PVA/CS/ $CeAlO_3$ nanofibers

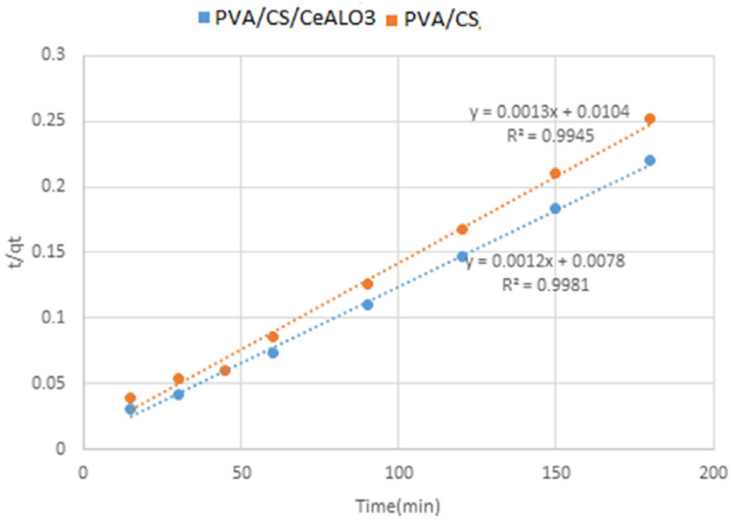

Fig. 11. Pseudo-second-order plot sorption of MB onto PVA/CS and PVA/CS/ $CeAlO_3$ nanofibers

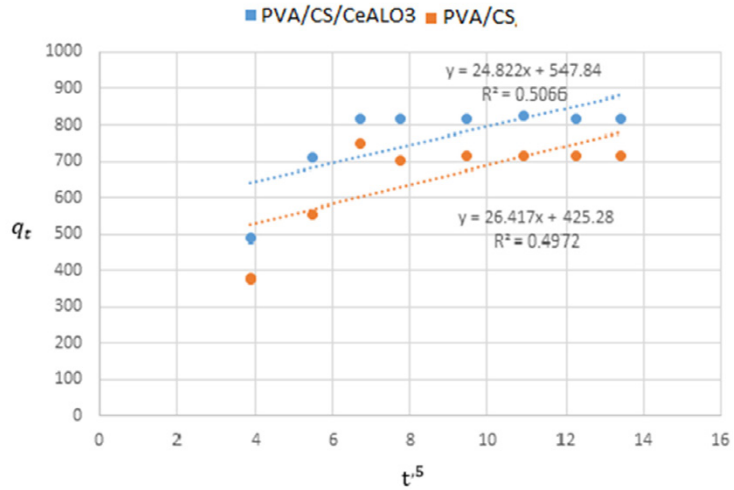

Fig. 12. intraparticle diffusion plot sorption of MB onto PVA/CS and PVA/CS/ $CeAlO_3$ nanofibers

experimental q_e value (714.61) when compared with the first-order model. The coefficient of determination (R^2) of the intraparticle diffusion model reflected a poor fit to the experimental equilibrium data for both adsorbents compared to the other models. The adsorption of MB by improved and net nanofibers can thus be considered following second-order kinetic models.

Effect of initial concentration

The effect of MB initial concentration in the range of 400 to 600 mg/L was investigated. According to the results, the uptake capacity value increased from 816.05 to 906.05 and from 714.61 to 800 by increasing initial concentration for improved and net nanofibers, respectively. This could be due to the increased driving force of mass transfer at higher concentrations of MB.

Isotherm of sorption

Isotherm models can describe the relationship between the amount of dye adsorbed on the external surface of the adsorbent and the dye content remaining in the solution. The results of the experiments were analyzed using two well-known isotherm models of Langmuir and Freundlich. The Langmuir isotherm is based on monolayer adsorption on the surface of the adsorbent, while

Table 2. sorption isotherm parameters for the MB removal by different sorbents

Sorbent	Langmuir constants				Freundlich constants		
	$b\ (\frac{1}{mg})$	R_L	$Q°\ (\frac{mg}{g})$	R^2	$k_f\ (mg/g)$	$_n{}^{-1}$	R^2
PVA/CS nanofibers	0.006	0.294	1111	0.97	121.51	0.31	0.96
PVA/CS/ $CeAlO_3$ nanofibers	0.015	0.142	1000	0.98	298.86	0.18	0.99

Table3. Comparison of the maximum adsorption capacities of MB dye onto various adsorbents

Adsorbents	Q_{max} (mg/g)	References
Magnetic fish scale	60.87	25
Peanut hull	68.03	26
Walnut sawdust	59.17	27
Magnetic modified MWCNT	48.10	28
Rice husk	40.59	29
Nanomagnetic manganese oxide	35.40	30
Magnetic MWCNT	15.74	31
Fine grinded wheat straw	2.23	32
Wood waste activated carbon	4.937	33
Walnut wood activated carbon	18.51	34
Peanut stick activated carbon	2.54	35
Albizia lebbeck seed pods Activated carbon	328.30	36
Bone charcoal	5.00	37
Fe3O4 NPs	45.40	38
Gold nanoparticles loaded on activated carbon	185.10	39
Calcium alginate/bentonite/activated carbon	994.06	40
Cu@ Mn-ZnS-NPs-activated carbon	72.93	41
nano-porous modified Na-bentonite	294.00	42
Fe3O4/AC nanocomposite	384.60	43
PVA/CS electrospun nanofibers	714.61	This study
PVA/CS/ $CeAlO_3$ electrospun nanofibers	817.81	This study

the Freundlich model investigates the multilayer adsorption on the surface of the adsorbent. Equations 5 and 6 represent the linear form of the adsorption isotherm [26].

$$\frac{1}{qe}=\frac{1}{Q°}+\frac{1}{bQ°Ce} \quad (5)$$

$$ln\ q_e = ln\ k_f + \frac{1}{n}\ lnc_e \quad (6)$$

Where, c_e is Equilibrium concentration, (mg / L) q_e adsorption capacity at equilibrium, (mg / g) Q ° equal to the maximum amount of adsorbed dye per gram of adsorbent in the Langmuir equation, k_f Freundlich isotherm model capacity, and n is the amount of adsorption capacity in Freundlich equation. Using these equations and matching them with the equations of adsorption isotherm, the parameters of the adsorption isotherm were calculated (Table 2). Furthermore, if the R_L value (the dimensional factor) be in the range of $0 < R_L < 1$, the adsorption process will favorable (26).

$$R_L = \frac{1}{1+bc_0} \quad (7)$$

According to the obtained high values of R^2, it can be found that there is a good correlation between the obtained data and the adsorption isotherm. Therefore, the adsorption equilibrium fits the Freundlich and Langmuir isotherms on the improved nanofibers. The levels of n^{-1} and R in both adsorbents are in the desired range between 0 and 1, and therefore the Langmuir and Freundlich

models are suitable for investigating the adsorption process. A similar result can be seen in the research of Staroń et al. [27]. Also, the value of n is higher than 1 representing favorable adsorption. Thus, the prepared nanocomposite has high efficiency in removing MB dye.

Table 3 shows the comparison of the maximum adsorption capacity of various adsorbents to adsorbents used in this study. Both adsorbents seem to have lower uptake capacity than calcium alginate–bentonite–activated carbon and larger adsorption capacity than other adsorbents.

CONCLUSIONS

In this study CS/$CeAlO_3$ based nanocomposite, a new adsorbent was synthesized by electrospinning process and characterized. We used the Design expert software to find the best conditions for the synthesis of nanofibers with smooth and uniform structure. According to the obtained results, fibers were prepared uniformly under only one condition at voltage 18 kv, distance to collector 10 cm, and feed rate of 0.3 cm^3 /h. Then, the removal of MB dye from solution using modified nanofibers was investigated in batch technique. The optimum process conditions for MB removal were pH 10, contact time 45 min, initial MB concentration 400 mg/L. The maximum adsorption capacity of MB was 817.81 and 714.61 mg/g onto improved and net nanofibers, respectively. The kinetics of MB adsorption on improved nanocomposite follows the pseudo-second-order model. Furthermore, the equilibrium data of it followed the Freundlich and Langmuir isotherms. The results revealed that this nanocomposite was effectively used for the removal of MB dye from the aqueous solution.

CONFLICTS OF INTEREST

The authors declare that there are no conflicts of interest regarding the publication of the manuscript.

REFERENCES

1. Adeogun AO, Ibor OR, Adeduntan SD, Arukwe A. Intersex and alterations in the reproductive development of cichlid, Tilapia Guineensis, from a municipal domestic water supply lake (Eleyele) in south western Nigeria. Science of the Total Environment. 2016; 541:372-382.
2. Wong A, Koutsogiannis Z, Greene S, & McIntyre, S. Acase of hemolysis and methemoglobinemia following amyl nitrite use in an individual with G6PD deficiency. Journal of Acute Medicine. 2013: 3: 23–25.
3. Ghaedi M, Ghazanfarkhani MD, Khodadoust S, Sohrabi N, Oftade M. Acceleration of methylene blue adsorption onto activated carbon prepared from dross licorice by ultrasonic: Equilibrium, kinetic and thermodynamic studies. Journal of Industrial and Engineering Chemistry. 2014;20(4):2548-60.
4. Bensalaha H, Bekheet M, Younssi S, Ouammou M, Gurlob A. Removal of cationic and anionic textile dyes with Moroccan natural phosphate. Journal of Environmental Chemical Engineering. 2017:5:2189-2199.
5. Haider S, Park S. Preparation of the electrospun chitosan nanofibers and their applications to the adsorption of Cu(II) and Pb(II) ions from an aqueous solution. Journal of Membrane Science. 2009: 328 :90–96.
6. Wnek G, Carr M, Simpson D, Bowlin G. Electrospinning of nanofiber fibrinogen structures, Nano Lett. 2003:3:213–216.
7. Zhang Y, Venugopal J, Huang Z, Lim C, Ramakrishna S. Crosslinking of the electrospun gelatin nanofibers, Polymer. 2006: 47:2911–2917.
8. Ma Z, Kotaki M, Ramakrishna S. Electrospun cellulose nanofiber as affinity membrane. Journal of Membrane Science. 2005:265:115–123.
9. Zhang Y, Ouyang H, Lim C, Ramakrishna S, Huang Z. Electrospinning of gelatin fibers and gelatin/PCL composite fibrous scaffolds, Journal of Biomedical Materials Research Part B.2005: 72:156–165.
10. Li M, Guo Y, Wei Y, MacDiarmid A, Lelkes P. Electrospinning polyanilinecontained gelatin nanofibers for tissue engineering applications. Biomaterials. 2006: 27:2705–2715.
11. Peesan M, Rujiravanit R, Supaphol P. Electrospinning of hexanoyl chitosan/ polylactide blends. Journal of Biomaterials Science, Polymer Edition. 2006:17: 547–565.
12. Mei Y, Runjun S, Yan F, Honghong W, Dou H, Chengkun L. Preparation, characterization and kinetics study of chitosan/PVA electrospun nanofiber membranes for the adsorption of dye from water. Journal of Polymer Engineering .2019:39: 459–471.
13. Mahmoodi N, Mokhtari-Shourijeh Z. Preparation of PVA-chitosan Blend Nanofiber and Its Dye Removal Ability from Colored Wastewater, Fibers and Polymers. 2015:16:1861-1869.
14. Mahmoodi MN, Oveisi M, Taghizadeh A, Taghizadeh M. Synthesis of pearl necklace-like ZIF-8@chitosan/PVA nanofiber with synergistic effect for recycling aqueous dye removal. Carbohydrate Polymers. 2020: 227:115364.
15. C.Y L, Lou T, Yan X, Long Y.Z, Cui G.P, Wang X.J. Fabrication of pure chitosan nanofibrous membranes as effective. International Journal of Biological Macromolecules. 2018:106:768–774.
16. birami A, Ahmadi S, Zarezadeh Mehrizi M, Beige R, Ghanavatian H. Synthesis of nanoparticles (CeAlO3) by soluble combustion technique, 6th international conference and exhibition on metallurgy and materials.1396. https://civilica.com/doc/699576.
17. Barati A, Asgari M, Miri T, Eskandari Z. Removal and recovery of copper and nickel ions from aqueous solution by poly (methacrylamide-co-acrylic acid)/ montmorillonite nanocomposites, Environmental Science and Pollution Research. 2013: 20:6242–6255.
18. Khairuddin E, Pramono S. B, Utomo V, Wulandari A, Zahrotul W, Clegg F. FTIR studies on the effect of

concentration of polyethylene glycol on polimerization of Shellac.: Conference Series.2016: 776 012053.
19. Irfan Khan M, Min T, Azizli K, Sufian S, Ullah H, Man Z. Effective removal of Methylene blue from water using Phosphoric acid based geopolymers. 2015: 5(75):61410-61420.
20. Tariqul Islam M, Saenz-Arana R, Hernandez C, Guinto T, Ariful Ahsan M, Kim H, Lin Y, Alvarado-Tenoriod B, Noveron J. Adsorption of methylene blue and tetracycline onto biomass-based material prepared by sulfuric acid reflux. RSC Advances. 2018; 8: 32545–32557.
21. Derakhshan Z, Baghapour M, Ranjbar M, Faramarzian M, Adsorption of Methylene Blue Dye from Aqueous Solutions by Modified Pumice Stone: Kinetics and Equilibrium Studies. Health Scope. 2013 ; 2(3):136-144.
22. Al-Ghouti M, Al-Absi R. Mechanistic understanding of the adsorption and thermodynamic aspects of cationic methylene blue dye onto cellulosic olive stones biomass from wastewater. Scientific Reports. 2020:10:15928.
23. Kazembeigi F, Arezoomand H, Faraji H, Mazloomi S, Mohammadi F, Moghadam F, Khoshneyat R, Nikonahad A, Nourmorai H. - Removal of Methylene Blue from Aqueous Solutions using Raw and Modified Rice Husk. The Veliger. 2014:53:1-7.
24. Shahverdi F, Ahmadi M, Avazmoghadam S, Faramarzi M.A. Comparative study of the kinetics and equilibrium of nickel(II) biosorption from aqueous solutions by free and immobilized biomass of Aspergillus awamori. Environmental Progress & Sustainable Energy. 2015;34: 1356–1364.
25. Barati A, Eskandari Z, Miri T, Asgari M. Removal of Fluoride Ion from Aqueous Solution by Nanocomposite Hydrogel Based on Starch/Sodium Acrylate/Nano Aluminum Oxide, Iranian Journal of Polymer Science and Technology.2013; 26: 381-391.
26. Shahverdi F, Ahmadi M, Avazmoghadam S. Isotherm models for the nickel(II) biosorption using dead fungal biomass of Aspergillus awamori: comparison of various error functions, Desalination and Water Treatment. 2016;57: 1–11.
27. Staroń P, Chwastowski J, Banach M. Sorption behavior of methylene blue from aqueous solution by raphia fbers. International Journal of Environmental Science and Technology. 2019; 16:8449–8460.
28. Gholami Ahmadgurabi N, Dadvand Koohi A, Ebrahimian Pirbazari A. Fabrication, Characterization, Regeneration and Application of Nanomagnetic $Fe^{3}O^{4}$@Fish Scale as a Bio-adsorbent for Removal of Methylene Blue. Journal of Water and Environmental Nanotechnology .2018: 3(3): 219-234.
29. Gong R, Ding Y, Li M, Yang C, Liu H, Sun Y. Utilization of powdered peanut hull as biosorbent for removal of anionic dyes from aqueous solution. Dyes and Pigments.2005;64(3):187-92.
30. Ferrero F. Dye removal by low cost adsorbents: Hazelnut shells in comparison with wood sawdust. Journal of Hazardous Materials. 2007:142(1-2):144-52.
31. Madrakian T, Afkhami A, Ahmadi M, Bagheri H. Removal of some cationic dyes from aqueous solutions using magneticmodified multi-walled carbon nanotubes. Journal of Hazardous Materials. 2011; 196:109-14.
32. Vadivelan V, Kumar KV. Equilibrium, kinetics, mechanism, and process design for the sorption of methylene blue onto rice husk. Journal of Colloid and Interface Science. 2005:286(1):90-100.
33. Chen H, Chu PK, He J, Hu T, Yang M. Porous magnetic manganese oxide nanostructures: Synthesis and their application in water treatment. Journal of Colloid and Interface Science. 2011:359(1):68-74.
34. Gao H, Zhao S, Cheng X, Wang X, Zheng L. Removal of anionic azo dyes from aqueous solution using magnetic polymer multi-wall carbon nanotube nanocomposite as adsorbent. Chemical Engineering Journal. 2013; 223:84-90.
35. Batzias F, Sidiras D, Schroeder E, Weber C. Simulation of dye adsorption on hydrolyzed wheat straw in batch and fixedbed systems. Chemical Engineering Journal. 2009:148(2-3):459-72.
36. Ghaedi M, Kokhdan SN. Removal of methylene blue from aqueous solution by wood millet carbon optimization using response surface methodology. Spectrochimica Acta Part A: Molecular and Biomolecular Spectroscopy. 2015; 136:141-8.
37. Ghaedi M, Mazaheri H, Khodadoust S, Hajati S, Purkait MK. Application of central composite design for simultaneousremoval of methylene blue and Pb2+ ions by walnut wood activated carbon. Spectrochimica Acta Part A: Molecular and Biomolecular Spectroscopy. 2015; 135:479-90.
38. Ghaedi M, Nasab AG, Khodadoust S, Rajabi M, Azizian S. Application of activated carbon as adsorbents for efficient removal of methylene blue: Kinetics and equilibrium study. Journal of Industrial and Engineering Chemistry. 2014;20(4):2317-24.
39. Ahmed MJ, Theydan SK. Optimization of microwave preparation conditions for activated carbon from Albizia lebbeck seed pods for methylene blue dye adsorption. Journal of Analytical and Applied Pyrolysis. 2014; 105:199-208.
40. Ghanizadeh G, Asgari G. Adsorption kinetics and isotherm of methylene blue and its removal from aqueous solution using bone charcoal. Reaction Kinetics, Mechanisms and Catalysis. 2010;102(1):127-42.
41. Ghaedi M, Hajjati S, Mahmudi Z, Tyagi I, Agarwal S, Maity A, et al. Modeling of competitive ultrasonic assisted removal of the dyes – Methylene blue and Safranin-O using Fe3O4 nanoparticles. Chemical Engineering Journal. 2015; 268:28-37.
42. Roosta M, Ghaedi M, Daneshfar A, Sahraei R, Asghari A. Optimization of the ultrasonic assisted removal of methylene blue by gold nanoparticles loaded on activated carbon using experimental design methodology. Ultrasonics Sonochemistry. 2014:21(1):242-52.
43. Benhouria A, Islam MA, Zaghouane-Boudiaf H, Boutahala M, Hameed BH. Calcium alginate–bentonite–activated carbon composite beads as highly effective adsorbent for methylene blue. Chemical Engineering Journal. 2015; 270:621-30.
44. Dastkhoon M, Ghaedi M, Asfaram A, Goudarzi A, Mohammadi SM, Wang S. Improved adsorption performance of nanostructured composite by ultrasonic wave: Optimization through response surface methodology, isotherm and kinetic studies. Ultrasonics Sonochemistry. 2017; 37:94-105.

45. Moradi N, Salem S, Salem A. Optimizing adsorption of blue pigment from wastewater by nano-porous modified Na-bentonite using spectrophotometry based on response surface method. Spectrochimica Acta Part A: Molecular and Biomolecular Spectroscopy. 2018; 193:54-62.

46. Ghasemi M, Mashhadi S, Azimi-Amin J. $Fe^{3}O^{4}$/AC nanocomposite as a novel nano adsorbent for effective removal of cationic dye: Process optimization based on Taguchi design method, kinetics, equilibrium and thermodynamics. Journal of Water and Environmental Nanotechnology. 2018: 3(4): 321-336.